JOURNAL OF MATERIALS SCIENCE 22 (1987) 4240–4246

Influence of the mode of synthesis on the morphology and structure of polyparaphenylene

P. PRADERE*, A. BOUDET
Laboratoire d'Optique Electronique du CNRS, 29 rue J. Marvig, BP 4347, 31055 Toulouse Cedex, France

The morphology and structure of pristine polyparaphenylene (PPP) have been investigated in detail using transmission electron microscopy techniques. A comparison is made between three samples prepared by the different polymerization techniques described by Kovacic, Yamamoto and Fauvarque. The morphology is either fibrillar or mosaic-like. The crystallinity, the size of crystallites and their relative orientation are different. The unit cells were indexed to be monoclinic. A single-crystal diffraction pattern is obtained for Yamamoto PPP, suggesting the presence of extended crystalline lamellae. This was confirmed by dark-field imaging where moiré patterns show the dimension of the lamellae (50 to 100 nm).

1. Introduction

Conductive polymers like polyacetylene (PA) and polyparaphenylene (PPP) have been extensively studied in the past few years because of their electrical properties obtained after doping with, for instance, strong oxidants such as arsenic pentafluoride (AsF_5). The high conductivities obtained after doping, associated with the lightness of these materials, would be of great interest for applications such as rechargeable batteries or light electrical conductors. Unfortunately, the doped material is unstable in air. One advantage of PPP, which is less conductive than PA after a maximum AsF_5 doping, is its better stability in air.

Polyparaphenylene (PPP) has received special attention since Shacklette *et al.* [1] discovered that its electrical conductivity could increase from 10^{-9} or 10^{-10} to $5 \times 10^4\ \Omega^{-1}\ m^{-1}$ when it is doped with AsF_5. This behaviour is similar to that of PA. However, the molecular structures of these two polymers are quite different so that the conduction mechanisms are probably not the same. A better knowledge of the detailed morphology and structure of PPP would allow one to judge critically the validity of the various conduction models. In this paper, we study the structure and the morphology of several PPP specimens, obtained by three different syntheses.

PPP can be synthesized in various different ways. The first synthesis, carried out in 1963 by Kovacic and co-workers [2, 3], consists in a polymerization of benzene using a Friedel–Crafts $AlCl_3$–$CuCl_2$ catalyst. More recently, Yamamoto and Yamamoto [4] have proposed a method involving polycondensation of a Grignard reagent formed when starting from dibromobenzene. In 1983, Fauvarque *et al.* [5] succeeded in obtaining PPP by electrosynthesis starting from dibromobenzene.

AsF_5-doped Yamamoto PPP is not as conducting as AsF_5-doped Kovacic PPP, although it has more linear chains [6]. The same conclusion was drawn for Fauvarque PPP.

Little information has been obtained in previous works on the structure and morphology of PPP. Froyer *et al.* [7] have observed a fibrillar morphology for Kovacic PPP, using scanning electron microscopy (SEM). With this technique, the resolution is limited by the 10 to 20 nm film of metal necessary to evaporate on the sample before imaging. Terakoa and Takahashi [8] have found different morphologies for Kovacic PPP using bright-field (BF) images and electron diffraction (ED) in transmission electron microscopy (TEM). No work has been done using dark-field (DF) imaging, although this technique gave us interesting preliminary results on the crystalline structure of Kovacic PPP and has been found successful in the study of PA [9]. Recently, Kawaguchi and Petermann [10] have reported an interesting study on the unit cell, using TEM.

Basic crystallographic results have nevertheless been obtained using X-ray [7, 11, 12] and neutron diffraction [13–15]. An accurate determination of the crystalline unit cell was not possible due to the poor crystallinity of the material. Two unit cells, monoclinic and orthorhombic are compatible with the diffraction patterns.

The advantage of TEM is to provide information on small sample areas (spatial resolution). However, this resolution is limited by radiation damage [16–18]. With this technique, we could observe new details concerning the structure and morphology of different PPP samples. Preliminary results have already been given in previous papers [19, 20].

2. Experimental procedure

Table I lists the different samples studied here. Each

* *Present address*: McGill University, Department of Chemistry, Pulp and Paper Building, 3420 University Street, Montreal, Québec H3A 2A7, Canada.

0022–2461/87 $03.00 + .12

TABLE I List of the samples

Kovacic		Yamamoto	Fauvarque
CNET (Lannion)	VTT (Helsinki)		
PPP K1	PPP K2	PPP Y	PPP F

of them consists of an insoluble and infusible powder. All the samples were kindly provided by G. Froyer from the CNET laboratory (Lannion, France) and H. Stubb from the VTT laboratory (Helsinki, Finland).

By light microscopy the powder granularity was measured to range from a few micrometres to about 50 μm. In order to obtain sufficiently thin samples suitable for TEM, the powder was dispersed in pure ethanol by ultrasonication. Drops of the suspension were then allowed to dry on a 10 nm thick carbon-coated grid.

TEM was carried out at 120 kV with a Philips EM 400 using a field-emission gun, and at 200 kV with a Jeol 200 CX. Radiation damage was minimized by using a low-dose technique and highly sensitive Kodak DEF-5 X-ray film. Minimization of radiation damage is critical in obtaining DF images due to the fact that less than 5% of the beam is used to form the image. Exposure times from 10 to 20 sec were used. The fading of the diffraction spots was found to be an exponential function of the dose, in agreement with theoretical calculations [18]. The critical dose, defined as the dose reducing the intensity of the most intense diffraction spot to 1/e of its initial value, was found to be 9000 C m^{-2} for Kovacik PPP and about 5000 C m^{-2} for the other two PPPs at 200 kV (room temperature). Consequently, only two or three consecutive DF images can be obtained from the same area with a sufficient resolution to discern the small crystallites in these thick specimens.

3. Morphology

In a recent paper we explored the typical fibre morphology of PPP K1 (Kovacic synthesis) [19]. Isolated fibres show a smooth and regular surface, with an average diameter of 40 $\pm$ 10 nm, although exceptions are seen, probably due to local variations in polymerization conditions. Other kinds of feature, such as flat film areas, have been observed, but they represent less than 1% of the material seen on the grid. Fig. 1, obtained from PPP K2, shows that the morphology is slightly modified when the polymerization conditions are different (samples prepared in another laboratory). Irregular fibres with rough surfaces sometimes disappear into larger unorganized areas.

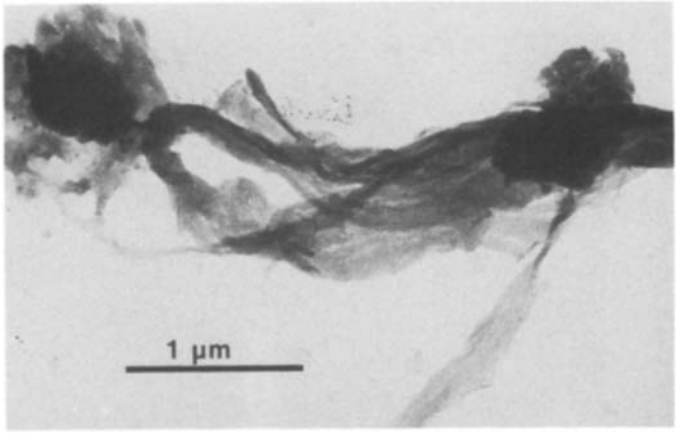

Figure 1 Morphology of PPP K2.

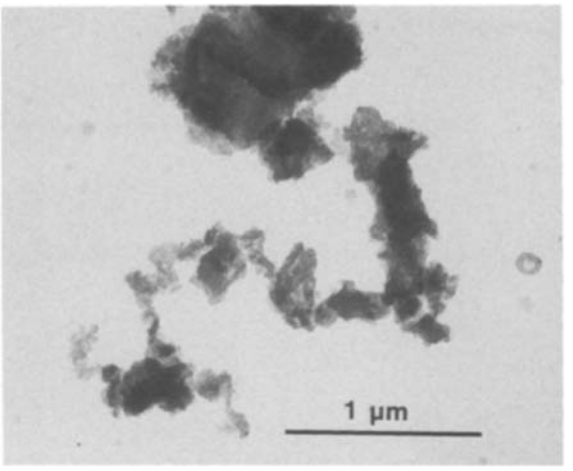

Figure 2 Granular morphology of PPP Y.

The great dependence of the morphology on the method of synthesis is illustrated by the totally different morphologies observed for PPP Y (Yamamoto synthesis) and F (Fauvarque synthesis). Fig. 2 is a BF image obtained from PPP Y. Small grains, 20 to 50 nm wide, are densely packed in larger aggregates of various sizes; the largest one does not reach 1 μm. The same kind of granular morphology is observed for PPP F. In this material, small grains of similar dimensions are packed together but here they build more homogeneous plate-like structures whose dimensions are of the order of one micrometre. Such plates have an irregular surface as can be seen in Fig. 3.

As previously discussed for PA, the morphology is very important to understand the diffusion of the dopant inside the material. In our case, the more compact granular morphology of PPP Y and PPP F could be an obstacle to the dopant diffusion. Indeed, these samples are slightly less conducting at the maximum doping concentration.

4. Crystalline structure

By combining diffraction patterns and DF images, we have examined the crystallinity, the unit cell, the crystallite shapes and the texture of the three types of sample.

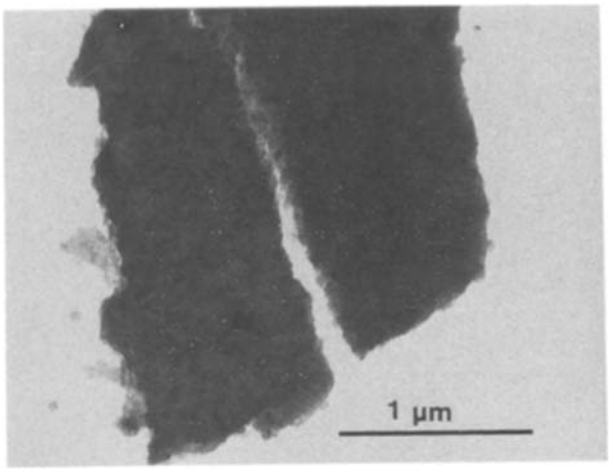

Figure 3 Plate-like structures observed for PPP.

4.1. Crystallinity

Fig. 4 shows typical ED patterns obtained from the three samples K1, Y and F. Only 3 to 8 Debye rings are clearly seen. That means that we are dealing with poorly ordered samples. PPP F, for which the rings are thin and intense, appears as the most crystalline one and PPP K is the least crystalline sample.

TABLE II Interplanar spacings measured for our samples (*strong, †weak)

hkl	Spacing (nm)			
	PPP K1	PPP K2	PPP Y	PPP F
100	0.456*	0.455*	0.453*	0.455*
200	0.400	–	0.394*	0.394*
210	0.324*	0.325*	0.322*	0.321*
120	0.260†	–	–	0.263
310	0.240	–	–	0.238
002	0.212	0.210	–	0.210
320	0.193†	–	–	0.191
420	0.161†	–	–	0.161

4.2. Unit cell

Table II displays the values of the lattice spacings measured for the different samples. The sharpness of PPP F reflections allowed us to determine the values accurately. Small differences from these values are observed for the other samples, for instance in the 200 reflection in PPP K1. However, these differences are not significant since the lattice spacings are not as accurate as those of PPP F, due to the width of the reflections in these samples. Furthermore, as seen from Table III which displays other authors' results, these values are similar to Kovacic's original results.

The limited number of reflections allows the structure to be modelled by either a monoclinic or an orthorhombic unit cell. We have indexed the reflections using a monoclinic unit cell with parameters $a = 0.806 \pm 0.010$ nm, $b = 0.555 \pm 0.004$ nm, $c = 0.430 \pm 0.004$ nm, $\beta = 100°$.

The monoclinic model is strongly supported by consideration of the length of the phenyl ring, by analogy with the oligomers and by the shape of the 002 reflection. It can be seen in Fig. 5, which shows a diffraction pattern from a PPP K isolated fibre, that the 002 reflection is far more angularly extended than $hk0$ reflections. This spreading is attributed to the overlapping of two 002 arcs, obtained by rotation

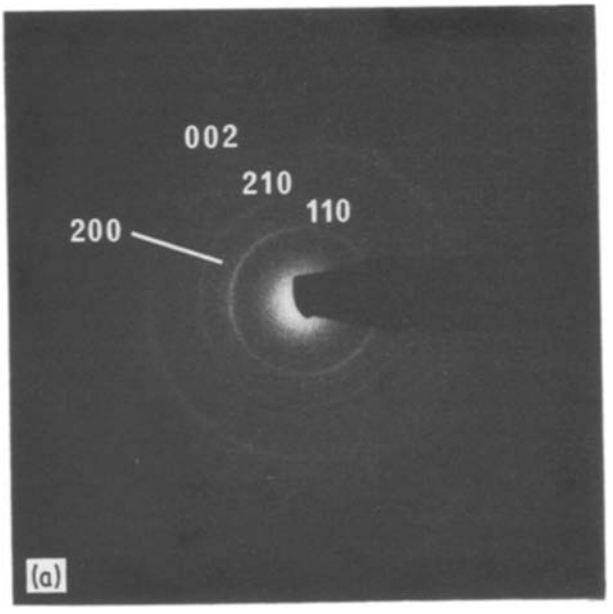

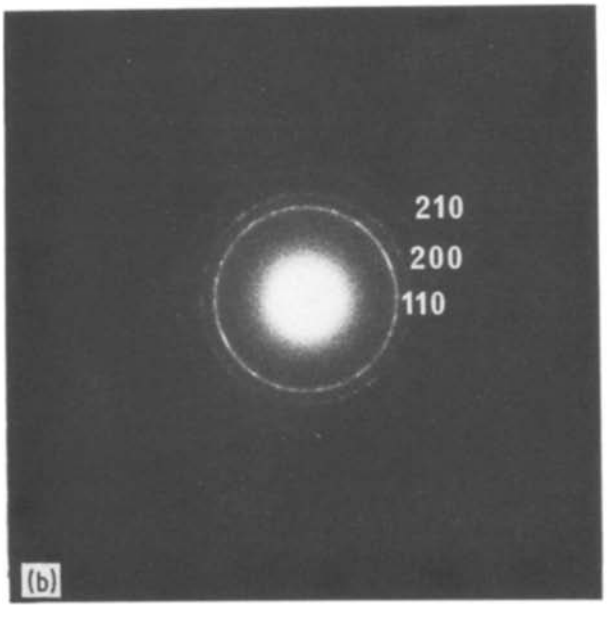

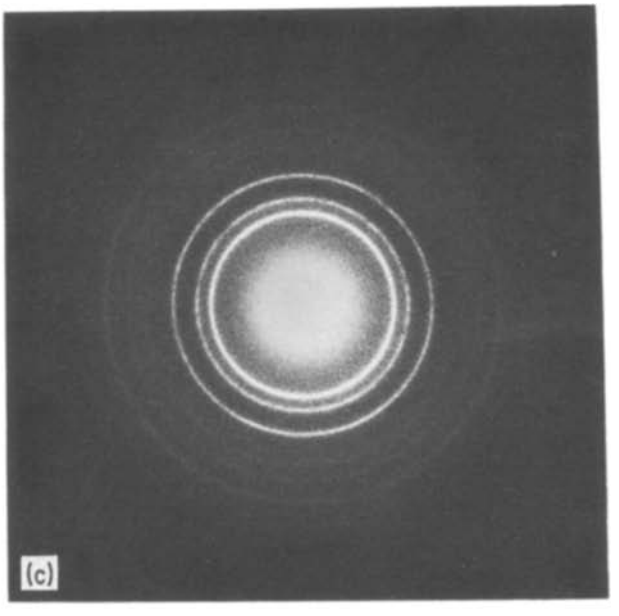

Figure 4 Typical ED pattern obtained from (a) PPP K (K1 and K2 give the same pattern), (b) PPP Y, (c) PPP F.

TABLE III Lattice spacings from the literature

h k l	Spacing (nm)		
	Kovacic [21] (X-rays)	Hasslin [15] (neutrons)	Kawaguchi [10] (electrons)
1 0 0	0.453	0.447	0.452
2 0 0	0.391	0.386	0.390
2 1 0	0.319	0.316	0.318
1 2 0	0.260	–	0.260
3 1 0	0.235	0.232	0.232
0 0 2	0.210	0.210	0.2105
3 2 0	0.189	0.195	0.186
4 1 0	0.183	–	–
4 2 0	0.159	0.158	0.156

around the c axis as shown in Fig. 6. The angle between the c and c^* axes is $(\beta - \pi/2)$. The β value cannot be rigorously evaluated because the visible spreading of the reflection on the film is influenced by the optical density of the reflection itself. This density is in turn related to the reflection intensity in reciprocal space by the Lorentz factor which is unknown for the 0 0 1 reflections. If we neglect the correction by the Lorentz factor, we find very approximately $\beta \approx 100°$. What is significant here is not the value of β but the fact that it is different from 90°.

The length of a phenyl ring has been evaluated to be 0.430 nm in p-terphenyl and 0.434 nm in *p*-quaterphenyl [22, 23]. The distance between the 0 0 1 planes was found to be 0.422 nm. This distance cannot accommodate a chain axis normal to these planes, but instead corresponds to a phenyl ring tilted by an angle of 11 to 14°. This structure is then analogous to the chain packing described in all oligomers (molecules tilted by an angle of 15° with respect to the (a, b) plane) which provides further evidence supporting the monoclinic unit cell.

This result is in disagreement with the opinion of Kawaguchi and Petermann [10], who proposed an orthorhombic unit cell. They claimed that the 0 0 2 reflection is not split into two spots as would be expected for a monoclinic unit cell, and that the d_{002} value is shifted by overlapping of the 0 0 2 reflection with a possible 1 0 2 or 0 1 2 reflection. Both these possibilities seem unlikely since, first, we are dealing with arcs, not diffraction spots, even in the case of an area of dimensions as small as 40 nm (the crystallite size is less than 5 nm). Furthermore, in the diffraction pattern of an oriented fibre, the 1 0 2 or 0 1 2 reflections are far enough from the 0 0 2 one so that overlapping would be clearly discriminated on the pattern of Fig. 5 (compare Figs 5 and 6).

Nevertheless, we agree with these authors on one point: another reason for the spreading of the 0 0 2 reflection can be the second-order distortions (paracrystalline structure) [24]. This should be the sole cause of the spreading in the models based on an orthorhombic unit cell as proposed by Kawaguchi and Petermann, but not in the case of a monoclinic unit cell. We cannot exclude the existence of paracrystalline distortion, as it is likely for such a poorly ordered crystalline material; however, it is our opinion that this distortion coexists in conjunction with an average monoclinic unit cell, as evidenced by the data pertaining to the length of the phenyl ring.

In this view, the theoretical crystalline density ϱ_{cr} is found to be 1.33 g cm^{-3}, with two chains present in the unit cell.

4.3. Crystallite shape and texture

DF imaging is a much more precise technique to determine the crystallite dimensions in comparison with the estimate given by measuring the broadening of the diffraction maxima in X-ray diffraction patterns. Especially in our case, the PPP lattice is subject to distortions like paracrystalline disorder [24, 25] that can affect the width of the diffraction peaks and lead to underestimation of the size.

We have previously shown [19] that crystallites in PPP K1 are very small, approximately 4 nm wide in a direction normal to the chain axis. Furthermore, all the crystallites have their c axis (chain axis) approximately parallel to the fibre axis. This fact reflects the unidimensional character of the material and should

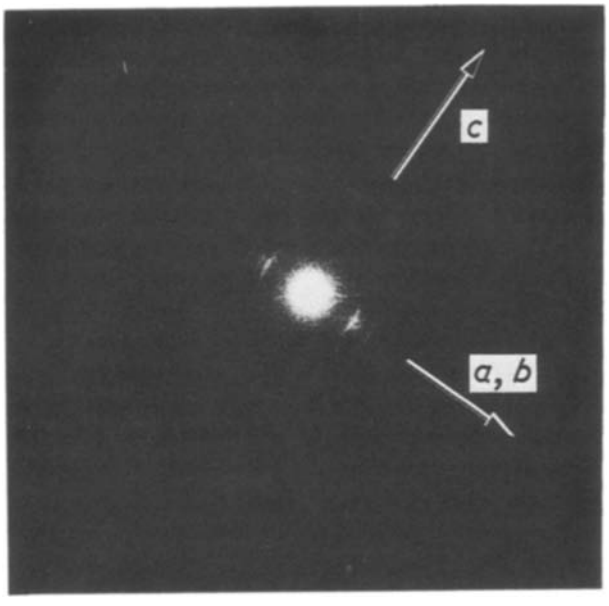

Figure 5 Electron diffraction pattern from a straight isolated fibre of PPP K1.

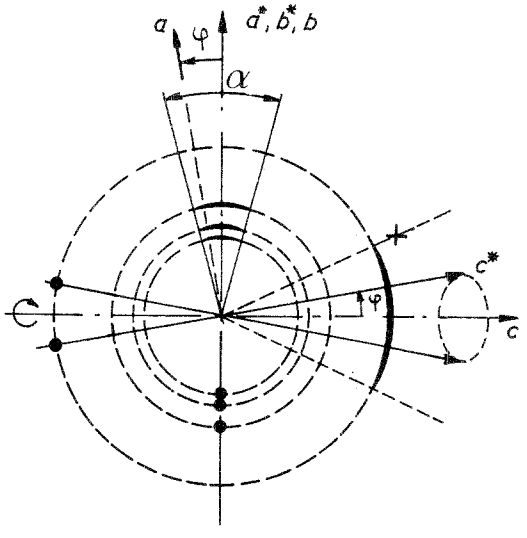

Figure 6 Model for a monoclinic unit cell. Dots represent diffraction spots which are in fact spread into arcs due to a dispersion α in the chain axis orientation. Reflections shown are 1 1 0, 2 0 0, 2 1 0 and 0 0 2. The cross shows the position of a possible 1 0 2 or 0 1 2 reflection. $\phi = \beta - \pi/2$.

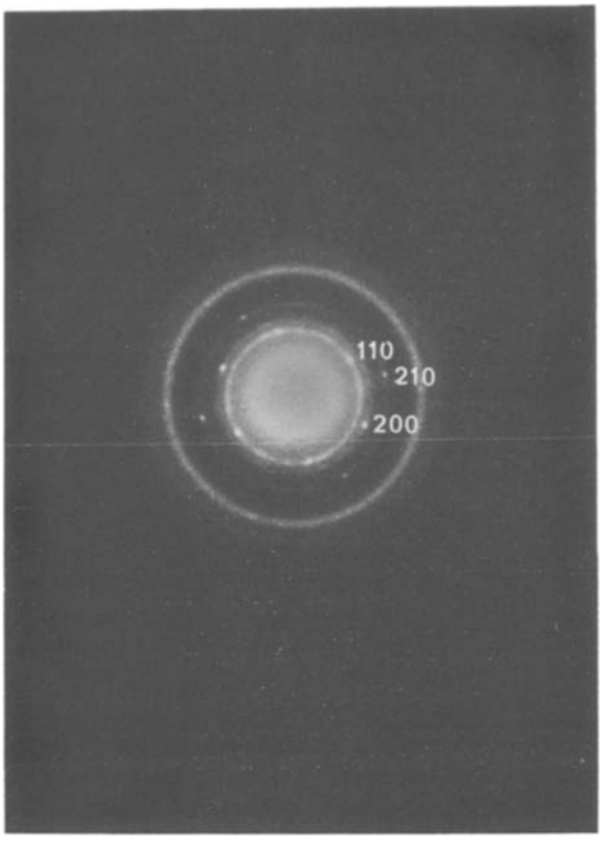

Figure 7 ED pattern of a single crystal of PPP Y. Debye rings result from the deposition of a thin layer of gold on to the sample for camera length calibration.

be taken into account when explaining its electrical properties.

An interesting feature of the crystalline structure of PPP Y is the single-crystal diffraction pattern shown in Fig. 7. The indexating of this pattern shows that within the crystal the chains lie parallel to the electron beam. This pattern reveals evidence for the existence of crystalline platelets extended in a direction normal to the chain axis. The small length and the linearity of the chains in PPP Y can explain the formation of larger crystallites compared with PPP K1.

The existence of large crystallites in PPP Y, but also in PPP F, is confirmed by DF imaging. Fig. 8 was obtained for PPP F by selecting the 1 1 0 and 2 0 0 reflections with a $0.5\,nm^{-1}$ diameter aperture in the diffraction plane. It shows that many crystallites have a rod-like shape with an average length of 20 nm. The

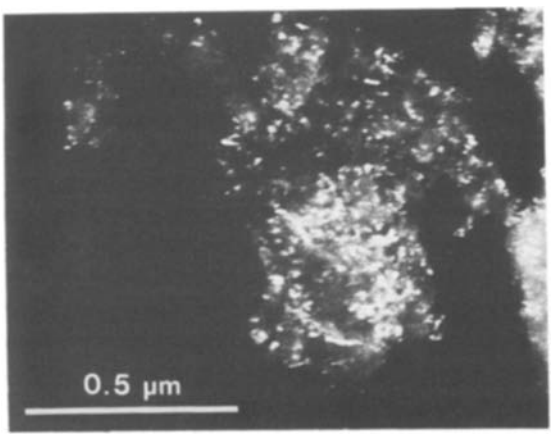

Figure 8 DF image of PPP F showing large elongated crystallites.

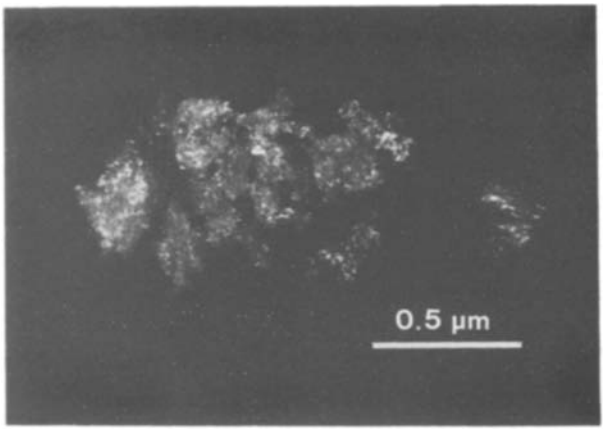

Figure 9 DF image of PPP Y: crystallites of various sizes, from 5 to 30 nm, are seen.

short width may result from the fact that the average chain length is only about 20 monomers (6 nm). Large crystallites, up to 30 nm long, are also seen for PPP Y (Fig. 9) and their elongated shape in some cases strongly supports the hypothesis of a lamellar structure.

This is confirmed in some DF images, in which many fringes can be seen for PPP Y as well as for PPP F. These fringes (see Figs 10a and c) were interpreted as moiré patterns. They were commonly seen throughout the specimen. Fringe spacing varies depending on their relative orientation with respect to the selected diffraction vector. When the fringes are parallel to this vector the spacing is in the range between 1.5 and 7 nm. When the fringes are perpendicular, the spacing is always 3 nm. When the angle is about 45° (Fig. 10c) the spacing is 2 nm. These three cases correspond to three kinds of moiré pattern resulting from the overlapping of two lamellar crystals having their c axis normal to their surface: rotation moiré, parallel moiré and mixed rotation–translation.

The formation of a rotation moiré pattern results from the interference of two 1 1 0 or 2 0 0 diffracted beams from two overlapping crystals rotated by an angle δ with respect to each other. In this case the fringe spacing is given by the formula

$$D = \frac{1}{|\Delta \boldsymbol{g}|} = \frac{d_{hkl}}{\delta} \qquad (1)$$

The particular objective aperture we have used to select 1 1 0 and 2 0 0 reflections limits the largest value of δ to 25°; thus the minimum interfringe distance is 1.3 nm. This agrees well with the minimum interfringe distance of 1.5 nm that we observed.

Another type of moiré pattern (parallel moiré) results from the interference between a 1 1 0 reflection from one crystal and the 2 0 0 reflection from another, when these crystals are stacked with the two sets of planes parallel. In this case the fringe spacing is given by

$$D = \frac{1}{|\Delta \boldsymbol{g}|} = \frac{1}{(1/d_{110}) - (1/d_{200})} \approx 3\,nm \qquad (2)$$

This value agrees well with our observations on fringes that were oriented normal to $\boldsymbol{g}$.

Finally, observation of oblique fringes are also

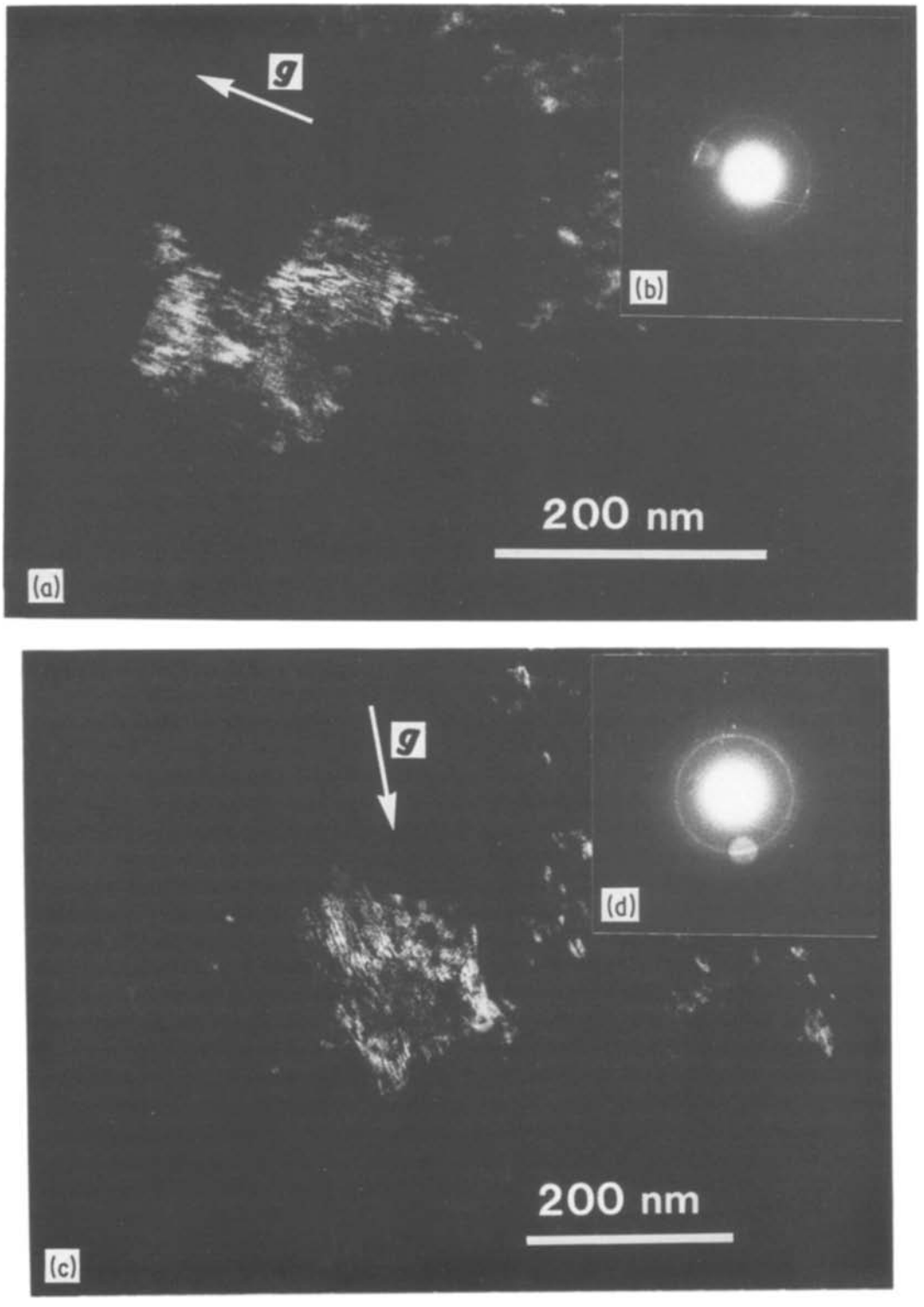

Figure 10 Moiré fringes suggesting an overlapping of lamellar crystals: (a) PPP Y, (b) corresponding diffraction pattern showing the beam selected by the objective aperture to form the dark field; (c) PPP F, (d) its diffraction pattern.

in agreement with a mixed moiré pattern that occurs when the two previous sets of planes are slightly rotated by an angle β, so that the spacing is given by

$$D = \frac{1}{|\Delta \boldsymbol{g}|} = \frac{\sin \beta}{(1/d_{110}) - (1/d_{200})} \quad (3)$$

where β is the angle between the fringes and $\boldsymbol{g}$. For $\beta = 45°$, $D = 2.1$ nm, in agreement with our observations.

From these results, we deduce that large crystalline lamellae exist in PPP F and Y. The small lamellae are directly imaged in DF pictures. The larger ones stack together and give rise to moiré patterns which extend up to 60 nm.

4.4. Relationship between structure and electrical properties

An interesting feature to consider is the maximum d.c. conductivities measured for the three samples after total AsF_5 doping: $270\,\Omega^{-1}\,cm^{-1}$ for PPP K1, $4\,\Omega^{-1}\,cm^{-1}$ for PPP Y and $25\,\Omega^{-1}\,cm^{-1}$ for PPP F. (These conductivities were measured by G. Froyer and co-workers in the CNET laboratory, Lannion, France [6, 25].) It is obvious that PPP K1, which has

TABLE IV Main results for the structure and morphology of PPP, comparing the three different syntheses

	Synthesis		
	Kovacic	Yamamoto	Fauvarque
Morphology	Entangled fibres of diameter 40 nm. Globular structures.	Grains ($\leqslant 50$ nm) agglomerated in clusters of various sizes.	Grains, plate-like structures up to 1 μm long.
Unit cell	Monoclinic: $a = 0.806$ nm, $b = 0.555$ nm, $c = 0.430$ nm, $\beta = 100°$		
Texture	Crystallites 4 nm. Orientation with c axis along the fibre.	5 to 30 nm	Large crystallites 20 nm Lamellar crystals (chains normal to surface), stacked when their size is over 20 nm.

the lowest crystallinity and less linear chains, is the best conductor. Therefore crystallinity and chain linearity do not seem to be predominant factors in the conductivity. On the other hand all the chains are parallel inside a fibre. This supports a conduction model such as the one proposed by Bredas *et al.* [26, 27] in which conductivity is explained by jumps of mobile bipolarons between parallel chains.

5. Conclusion

Table IV sums up the characteristics of the three kinds of PPP sample. PPP F, electrochemically polymerized, appears to be the most crystalline one, containing large, regular, lamellar crystallites, the thickness of which is limited by the short length of the molecular chains. PPP Y has a similar texture, related to the linearity of the chains, but the polymerization mode leads to a larger dispersity. PPP K is the least crystalline one but has the distinction of being made of fibres in which the crystallites are oriented along the fibre axis.

The unit cell for all three types was determined to be monoclinic, with parameters $a = 0.806$ nm, $b = 0.555$ nm, $c = 0.430$ nm, $\beta = 100°$ and the theoretical density $\varrho_{cr} = 1.33\,g\,cm^{-3}$. The crystallinity is not perfect and is likely to be distorted in a paracrystalline manner.

The unidimensional character of the material is underlined by the higher conductivities obtained after a maximum doping on PPP K, for which all the molecular chains are parallel inside the elementary fibres of its morphology. Preliminary experiments have shown that the morphology is not drastically changed after doping. The evolution of the structure after doping will be discussed in another paper [28].

Acknowledgement

We thank G. Froyer, F. Maurice and J. Y. Goblot for providing most of the samples, and for their kind help. We thank Dr E. L. Thomas for pertinent remarks.

References

1. L. W. SHACKLETTE, R. R. CHANCE, D. M. IVORY, G. G. MILLER and R. H. BAUGHMAN, *Synth. Met.* **1** (1979) 307.
2. P. KOVACIC and A. KYRIAKIS, *J. Amer. Chem. Soc.* **85** (1963) 453.
3. P. KOVACIC and J. OZIOMEK, *J. Org. Chem.* **29** (1964) 100.
4. T. YAMAMOTO and A. YAMAMOTO, *Chem. Lett. (Chem. Soc. Jpn)* (1977) 353.
5. J. F. FAUVARQUE, M. A. PETIT, F. PFLUGER, A. JUTAND, C. CHEVROT and M. TOUPEL, *Makromol. Chem. Rapid Commun.* **4** (1984) 455.
6. G. FROYER, J. Y. GOBLOT, J. L. GUILBERT, F. MAURICE and Y. PELOUS, *J. Physique Coll. C3* **44** (1984) 745.
7. G. FROYER, F. MAURICE, J. P. MERCIER, D. RIVIERE, M. Le CUN and P. AUVRAY, *Polymer* **22** (1981) 992.
8. F. TERAKOA and T. TAKAHASHI, *J. Makromol. Sci. Phys. B* **1** (18) (1980) 73.
9. J. C. W. CHIEN, "Polyacetylene" (Academic, New York, 1984).
10. A. KAWAGUCHI and J. PETERMANN, *Mol. Cryst. Liq. Cryst.* **133** (1986) 189.
11. L. W. SHACKLETTE, H. ECKHARDT, R. R. CHANCE, G. G. MILLER, D. M. IVORY and R. H. BAUGHMAN, *J. Chem. Phys.* **73** (1980) 4098.
12. P. KOVACIC, M. FELDMANN, J. P. KOVACIC and J. P. LANDO, *J. Appl. Polym. Sci.* **12** (1968) 1735.
13. M. STAMM, J. HOCKER and A. AXMANN, *Mol. Cryst. Liq. Cryst.* **77** (1981) 125.
14. M. STAMM and J. HOCKER, *J. Physique Coll. C3* **44** (1983) 667.
15. H. W. HASSLIN and C. RIECKEL, *Synth. Met.* **5** (1982) 37.
16. A. BOUDET and L. P. KUBIN, *Ultramicroscopy* **9** (1982) 409.
17. A. BOUDET and C. ROUCAU, *J. Physique* **46** (1985) 1571.
18. A. BOUDET, *ibid.* **47** (1986) 1043.
19. A. BOUDET and P. PRADERE, *Synth. Met.* **9** (1984) 491.
20. P. PRADERE, A. BOUDET, J. Y. GOBLOT, G. FROYER and F. MAURICE, *Mol. Cryst. Liq. Cryst.* **118** (1985) 277.
21. P. KOVACIC, M. FELDMANN, J. P. KOVACIC and J. P. LANDO, *J. Appl. Polym. Sci.* **12** (1968) 1735.
22. J. L. BAUDOUR, H. CAILLEAU and W. B. YELON, *Acta Crystallogr. B* **33** (1977) 1773.
23. Y. DELUGEARD, J. DESUCHE and J. L. BAUDOUR, *ibid.* **32** (1976) 702.
24. R. HOSEMANN and S. N. BAGCHI, "Direct analysis of diffraction by matter" (North-Holland, Amsterdam, 1962).
25. G. FROYER, private communication.
26. J. L. BEDAS, R. R. CHANCE and R. SILBEY, *Mol. Cryst. Liq. Cryst.* **77** (1982) 319.
27. *Idem, ibid. Phys. Rev. B* **26** (1982) 5843.
28. P. PRADERE and A. BOUDET, *J. Mater. Sci. Lett.* in press.

Received 24 October 1986
and accepted 27 April 1987